# Maxwell-Bloch Turbulence

Kensuke IKEDA, Kenju OTSUKA* and Kenji MATSUMOTO**

*Research Institute for Fundamental Physics, Kyoto University, Kyoto 606*
**NTT Basic Research Laboratories, Musashino, Tokyo 180*
***Faculty of Pharmaceutical Sciences, Hokkaido University, Sapporo 060*

Turbulent state of the Maxwell-Bloch (M-B) equation, a classical model describing propagation of light through active resonant medium, is investigated in detail for a large number of cavity modes. The M-B system has turbulent solutions corresponding to the multi-mode laser oscillation. Confining ourselves to the good cavity case, the nature of the turbulent solution is studied in detail with use of the method of information theoretical characterization in the wave-number domain. How the networks of information carried by turbulent disturbances are formed in the wave-number domain is clarified. Turbulent disturbances are generated in relatively narrow wave-number regions which we call the Rabi chaotic bands and propagate towards various other regions in the wave-number space. In this way the wave-number space is classified into two domains, that is, the attractor interior and the attractor exterior. The information theoretical analysis further reveals that the resonant wave-number region is dynamically correlated with the Rabi chaotic bands on a time scale much longer than that of chaotic motion. Such a correlated motion is responsible for the slow dynamics in the resonant region to which most of photon energy is distributed. In particular two typical dynamical phenomena, i.e., the mode partition noise and the mode hopping often observed in multi-mode laser oscillation are self-induced in the resonant region. The mode hopping is a 'chaotic itinerancy' among the ruins of local attractors with simple topological characteristics. It is shown that the interplay between the resonant region and the Rabi chaotic bands yields a quite ingenious mechanism which enables the topological characteristic to change and thereby induces the mode hopping.

## Contents

## § 1. Introduction

An aim of the study of dissipative chaos is to elucidate the structure of complex dynamics of turbulent phenomena to which a huge number of degrees of freedom contribute. Fluid systems provide classical examples which exhibit such a complex turbulent dynamics. Besides the fluid systems, examples of turbulent behaviors have been found in various systems such as biological oscillations, chemical reaction systems, liquid crystals, nonlinear optical systems and so on.

From the standpoint of nonlinear dynamics, the nonlinear optical systems have the following attractive features : Most of the nonlinear optical systems can approximately be regarded as spatially one dimensional systems which are extended in the direction of the propagation of electromagnetic field, and the longitudinal modes alone contribute to the system's operation. Therefore, dynamics of nonlinear optical systems will much more easily be analyzed than other systems such as fluid systems. In spite of the simple structure, various complex dynamical phenomena have been observed in nonlinear optical systems. In particular a number of experimental studies have been reported for various kinds of fluctuation phenomena inherent in laser oscillation, for example, random spiking of laser output,[1] mode hopping,[2] construction and/or destruction of mode locking,[3] reflection induced noise[4] and so on. Most of these phenomena are related with the multi-mode laser oscillation where a number of longitudinal electromagnetic field modes participate in laser operation. In this sense the nonlinear optics is a 'store-house' of spatially one dimensional complex dynamical phenomena, and we may expect that various examples of one dimensional complex dynamics may be realized with the nonlinear optical systems. It should be, however, commented that additional spatial dimensions must be taken into account in order to describe the systems for which the transversal effect plays a crucial role. A typical example is the holographic laser which operate as an associative memory element.[5]

Multi-mode oscillation has extensively been investigated for passive nonlinear optical systems modeling the bistable optical elements.[6~10] However, the studies of complex dynamical behaviors in active nonlinear optical systems typically exemplified by lasers have been so far restricted to *low dimensional chaos* to which only a few number of longitudinal modes contribute,[8),10),11] although multi-mode oscillations are quite common in laser operations. Needless to say, this is because there has not been presented any efficient method by which the underlying structure of complex multi-mode dynamics can be analyzed. Recently an information theoretical method is proposed by two of the present authors[12] in order to characterize high-dimensional chaotic behaviors,[9] and the method has been applied to the study of the multi-mode oscillation described by a simplified model of passive optical resonators.[12] We expect that this method may successfully be applied to exper-

imental as well as theoretical studies of multi-mode laser oscillations.

In the present paper we study a typical turbulent state exhibited by a simplest model of the laser system: (1) First, we introduce the homogeneously broadened Maxwell-Bloch (M-B) equation, which is well known as a classical model of the laser system. Typical instability discovered for the M-B system is reviewed, and we show that this equation has a turbulent solution corresponding to multi-mode oscillation well above the instability threshold. (2) Secondly, we investigate the dynamical structure of the chaotic multi-mode oscillation by means of the information theoretical method mentioned above. The 2-point and the 3-point mutual information are used for analyzing how the chaotic disturbances are generated and propagate in the wave-number space, and thereby the information structure as well as the information networks formed through the chaotic dynamics is elucidated. (3) Finally, we demonstrate that our chaotic multi-mode oscillation is accompanied by the two fluctuation phenomena well known as the mode partition noise and the mode hopping, which have been often observed in multi-mode laser oscillations. This is the first evidence that both the mode partition noise and the mode hopping can be self-induced by the chaotic dynamics inherent in the M-B system itself without introducing any noise source from the external world. An important role of a simple topological constraint inherent in the M-B system in realizing these fluctuation phenomena is discussed. In particular it is shown that the chaotic dynamics enables the system to form easy paths among the localized chaotic attractors and to itinerate over the 'ruins' of these attractors. The three subjects described above are presented in §§2~4, respectively. Section 5 is devoted to summarizing the complex dynamical behavior realized in the turbulent state of the M-B system.

## § 2. Turburent states of Maxwell-Bloch system

### 2.1. *Model system*

Multi-mode oscillations in laser systems have been observed for gas lasers and solid state lasers in which the effect of inhomogeneous broadening cannot be neglected.[13] As has been pointed out by Casperson, the inhomogeneous broadening severely influences the stability of the system even in the case of single mode operation.[14] In the case of multi-mode operation Mandel showed that the stationary lasing regime disappears in the inhomogeneously broadened limit.[15] In the present paper we do not, however, take into account the effect of inhomogeneous broadening. This is because multi-mode oscillations in laser system have not been understood theoretically at all even for homogeneously broadened limit. Dye-lasers and semiconductor lasers (and maybe quantum-well lasers) provide some examples of homogeneously broadened system which exhibit multi-mode oscillation. Quite interesting effects of inhomogeneous broadening will be investigated in future studies.

The simplest classical model of the homogeneously broadened laser systems is the Maxwell-Bloch (M-B) equations describing the motion of electromagnetic field propagating unidirectionally through a resonant two-level medium. The Maxwell-Bloch (M-B) system is described by the following set of partial differential equations:

$$\partial E(t,z)/\partial t + c\partial E(t,z)/\partial z = \kappa(P(t,z)-E(t,z)), \tag{2·1a}$$

$$\partial P(t,z)/\partial t = \gamma_2(-P(t,z)+E(t,z)W(t,z)), \tag{2·1b}$$

$$\partial W(t,z)/\partial t = \gamma_1\Big[-W(t,z)+\lambda+1-\frac{\lambda}{2}(E(t,z)P^*(t,z)+E^*(t,z)P(t,z))\Big]. \tag{2·1c}$$

Here $t$ and $z$ are time and space coordinates, respectively, and $c$ is the light velocity. $E(t,z)$ and $P(t,z)$ are complex variables which represent the envelopes of the electric field and of the polarization field, respectively, and $W(t,z)$ is a real variable standing for the population inversion field. Thus $E(t,z)$ means the electric field in the resonator, whereas $P(t,z)$, $W(t,z)$ represent the two-level medium field. $\gamma_2$ and $\gamma_1$ are the transversal and longitudinal relaxation rates of the medium. On the other hand $\kappa$ is the parameter characterizing the loss rate of the resonator, and $\lambda$ stands for the pumping power. According to Risken and Nummendal,[16] we have scaled all the variables by their stationary values, which can be easily checked from the fact that the stationary solution is given by $E(t,z)=P(t,z)=W(t,z)=1$. Since we suppose that the system is in a ring resonator, the periodic boundary condition must be imposed upon $E(t,z)$, $P(t,z)$ and $W(t,z)$:

$$E(t,z=0)=E(t,z=L), \quad \text{etc.}, \tag{2·2}$$

where $L$ is the length of the resonator. The periodic boundary condition enables us to expand the variables $E(t,z)$, $P(t,z)$ and $W(t,z)$ into Fourier series:

$$E(t,z)=\sum_q E(t,q)e^{ikz}, \tag{2·3}$$

where

$$E(t,q)=L^{-1}\int_0^L E(t,z)e^{-ikz}dz. \tag{2·3′}$$

The Fourier modes used for the expansion are often called the (longitudinal) cavity modes. The integer $q$, which specifies the mode number, is related to the wave number $k$ by $k=2\pi q/L$. Then the Maxwell-Bloch system is transformed into the coupled-mode equations as

$$\frac{d}{dt}E(t,q)=(-ick-\kappa)E(t,q)+\kappa P(t,q), \tag{2·1′a}$$

$$\frac{d}{dt}P(t,q)=-\gamma_2 P(t,q)+\gamma_2\sum_{q_1+q_2=q}E(q_1)W(q_2), \tag{2·1′b}$$

$$\frac{d}{dt}W(t,q)=-\gamma_1(W(t,q)-\lambda-1)-\frac{\lambda\gamma_1}{2}\times\sum_{q_1+q_2=q}[E^*(t,-q_1)P(t,q_2)+E(t,q_1)P^*(t,-q_2)]. \tag{2·1′c}$$

In this description the mode amplitude of electric field $E(t,q)$ oscillates with the mode frequency $\omega=ck=2\pi q/t_R$, where $t_R=L/c$ is the round trip time of light in the

resonator. If we retain only the terms with $q=0$, then Eqs. (2·1′a∼c) reduce to the single-mode Laser model which is equivalent to the well-known Lorenz equation. Recently, the Lorenz instability and chaos have been observed by Weiss and his coworkers with a far-infrared laser.[17]

We integrate numerically the M-B equations (2·1′a∼c) by using the pseudospectral method, taking 256 or 512 cavity modes into account. Efforts to obtain chaotic solution of the M-B equations have been made by Mayer et al., Lugiato et al. and Ogawa.[18] Their computations, however, have been restricted within a few number of modes analyses. The pseudospectral method enables a large number of modes simulation of the M-B equations. Instead of analyzing the original M-B system, Brunner et al. examined chaotic multi-mode oscillation of Lamb's equation.[19] However, Lamb's equation, which is derived from the M-B equations by a perturbation expansion method, is inapplicable to describing the multi-mode oscillation which is likely to occur in high-pumping regime.[20),*]

Roughly speaking, the multi-mode oscillation occurs on the condition that the mode spacing $2\pi/t_R$ is much smaller than the transversal relaxation time, namely

$$\gamma_2 \gg 2\pi/t_R \,. \tag{2·4}$$

It is easy to show that Eqs. (2·1′a∼c) have the following family of solutions in which only a single mode is excited

$$E(t, q')=\sqrt{1-(\Omega/\gamma_2)^2\lambda^{-1}}\, e^{-i\Omega t}\delta_{q',q} \,, \tag{2·5a}$$

$$P(t, q')=(1+i\Omega/\gamma_2)E(t, q') \,, \tag{2·5b}$$

$$W(t, q')=[1+(\Omega/\gamma_2)^2]\delta_{q',0} \,. \tag{2·5c}$$

Except for the resonant ($q=0$) solution, Eqs. (2·5a∼c) oscillate with the frequency $\Omega=\gamma_2 ck/(\gamma_2+\kappa)$. In this sense the above class of solutions is the limit cycle solutions, but we call them the *single-mode stationary solution* (SSS) because the intensity (or photon number) is invariant in time. All the SSSs are not, however, stable: Indeed Gerber and Bütticker showed that the solutions satisfying the 'nearly resonant' condition[21]

$$|\Omega| < C\gamma_2 \tag{2·6}$$

are stable, where $C$ is a numerical constant less than 1. The SSSs play important roles in the turbulent state of the M-B system as will be fully described in §4.

### 2.2. *Resonant Rabi instability*

Now let us discuss the instability peculiar to the homogeneously broadened M-B system which leads to the turbulent behavior. This can easily be achieved by the standard linear stability analysis as has been done by Risken and Nummendal[16] and by Graham and Haken.[22] Instead of repeating the details of the analysis here again,

*) By using the pseudospectral method, the original M-B system can be integrated numerically with the CPU time much shorter than the one required for integrating Lamb's equation, although the latter is a simplified version of the former. For pseudospectral method, see S. A. Orszag, Stud. Appl. Math. **50** (1971), 293.

we describe the physical mechanism of the instability. Although our description is not mathematically rigorous, it provides a clear physical picture of the instability.

Suppose that the amplitudes of the nonresonant ($q\neq 0$) modes are much less than that of the resonant ($q=0$) mode. Then we may neglect all the nonlinear coupling terms on the r.h.s. of Eqs. (2·1′b, c) other than the terms of the combinations $(q_1, q_2)=(0, q)$, $(q, 0)$ (for (2·1′b)) and $(q_1, q_2)=(0, q)$, $(q, 0)$, $(0, -q)$, $(-q, 0)$ (for (2·1′c)). Thus the M-B equations for the nonresonant mode can be written as

$$\dot{\hat{E}}_q=(-ick-\kappa)\hat{E}_q+\kappa\hat{P}_q\,, \tag{2·7a}$$

$$\dot{\hat{P}}_q=-\gamma_2\hat{P}_q+\gamma_2(E_0\hat{W}_q+\hat{E}_qW_0)\,, \tag{2·7b}$$

$$\dot{\hat{W}}_q=-\gamma_1\hat{W}_q-\gamma_1\lambda(E_0\hat{P}_q+P_0\hat{E}_q)\,, \tag{2·7c}$$

where $\hat{X}_q=(X(t, q)+X(t, -q)^*)/2$ $(X=E, P, W)$. Assuming $\gamma_1=\gamma_2=\gamma$ for the sake of simplicity and introducing the variables $\hat{Z}_q^{(\pm)}=(\hat{P}(t, q)\pm i\hat{W}(t, q)/\sqrt{\lambda})$, the above equations are rewritten as

$$\dot{\hat{E}}_q=(-ikc-\kappa)\hat{E}_q+\frac{\kappa}{2}(\hat{Z}_q^{(+)}+\hat{Z}_q^{(-)})\,, \tag{2·8a}$$

$$\dot{\hat{Z}}_q^{(\pm)}=\gamma\{-\hat{Z}_{-q}^{(\pm)}\mp i\sqrt{\lambda}E_0\hat{Z}_q^{(\pm)}\mp i\sqrt{\lambda}\hat{E}_q\hat{Z}_0^{(\pm)}\}\,. \tag{2·8b}$$

Here we have assumed $E_0$ and $P_0$ to be real. In the large limit of the pumping power ($\lambda\gg 1$) the variable $\hat{Z}_q^{(\pm)}$ oscillates with the frequency $\gamma\sqrt{\lambda}E_0$ because the second term is predominant on the r.h.s. of Eq. (2·8b). This oscillation is no more than the Rabi precession. Thus we may set $\hat{Z}_q^{(\pm)}=e^{\mp i\gamma\sqrt{\lambda}E_0t}\tilde{Z}_q^{(\pm)}$ where $\tilde{Z}_q^{(\pm)}$ are slowly varying parts. Then the response of the electric field component to the rapidly oscillating complex variable $\hat{Z}_q^{(\pm)}$ can be written as

$$\hat{E}_q=\frac{\kappa/2}{\mp i\gamma\sqrt{\lambda}E_0+ikc+\kappa}\hat{Z}_q^{(\pm)}\,.$$

Substituting this into the second term on the r.h.s. of Eq. (2·8b), the original dumping constant of the variables $\hat{Z}_q^{(\pm)}$ is renormalized to yield

$$\gamma\to\gamma\left\{1-\frac{\sqrt{\lambda}(\gamma\sqrt{\lambda}E_0\mp kc)/\kappa}{2[(\gamma\sqrt{\lambda}E_0\mp kc)^2/\kappa^2+1]}\right\}. \tag{2·9}$$

Here we replaced $\hat{Z}_0^{(\pm)}$ by its stationary value $1\pm i/\sqrt{\lambda}\approx 1$. This fact implies that the modes which resonate with the Rabi precession frequency and hence satisfy $\sqrt{\lambda}\gamma E_0\mp kc\sim O(\kappa)$ becomes unstable as the pumping power increases, and the renormalized dumping constant (2·9) becomes positive. Hence it is appropriate to call this instability the *resonant Rabi instability*. It is different from the Lorenz instability of the single-mode laser system which occurs only when the relaxation constants of the system satisfy the 'bad' cavity condition

$$\kappa>\gamma_1+\gamma_2\,. \tag{2·10}$$

This is because the single mode cannot resonate with the Rabi frequency. The

resonant Rabi instability occurs irrespective of the cavity being 'good' ($\kappa < \gamma_1 + \gamma_2$) or 'bad'.

Here we summarize the result of a rigorous linear stability analysis for the resonant ($q=0$) SSS: It is straightforward to carry out the linear stability analysis of Eqs. (2·1a~c): Let the deviations of $E(t, q)$, $P(t, q)$ and $W(t, q)$ from the stationary solutions be $e(t, q)$, $p(t, q)$ and $w(t, q)$. Assuming

$$e(t, q), p(t, q), w(t, q) \propto \exp(i\beta_q t), \tag{2·11}$$

the linearized equation of motion yields the characteristic equation of $\beta_q$ given by the following cubic and quadratic equations:

$$\beta_q{}^3 + (\gamma_1+\gamma_2+\kappa+ick)\beta_q{}^2 + [\gamma_1(\gamma_2+\kappa+\gamma_2\lambda)+(\gamma_1+\gamma_2)ick]\beta_q + 2\gamma_1\gamma_2\kappa\lambda + \gamma_1\gamma_2(1+\lambda)ick = 0, \tag{2·12a}$$

$$\beta_q{}^2 + (\kappa+\gamma_2+ick)\beta_q + i\gamma_2 ck = 0. \tag{2·12b}$$

Physically interpreted, the former cubic equation represents the coupled motion $W(t, z)$ with the amplitudes of $E(t, z)$ and of $P(t, z)$, whereas the latter one describes a linearly coupled motion of the phases of $E(t, z)$ and of $P(t, z)$.[16] The former coupled motion is responsible for the resonant Rabi instability. Indeed, from Eq. (2·12a) we see that the real part of a root becomes positive when the pumping power exceeds the threshold value

$$\lambda_{\text{th}} = 4 + 3x + 2\sqrt{4+6x+2x^2}, \tag{2·13}$$

at the critical wavenumber $k_R$ defined by

$$ck_R = \gamma_1\sqrt{(3\lambda x - x^2)/2}\{1 - 2\kappa/[\gamma_2(\lambda-2)-\gamma_1]\}, \tag{2·14}$$

where $x = \gamma_1/\gamma_2$. $\lambda_{\text{th}}$ is often called 'the second threshold' (the first threshold is that of lasing, i.e., $\lambda=1$). We call the corresponding mode number $K_R$ closest to $k_R/(2\pi/L)$ the *Rabi unstable mode number*. It is not difficult to show that the frequency $\text{Im}(\beta_{q=K_R})$ of the Rabi unstable mode coincides almost with the Rabi frequency.

Whether the cavity is 'good' or 'bad' much influences not only the properties of instability but also those of the turbulent state which emerges far beyond the second

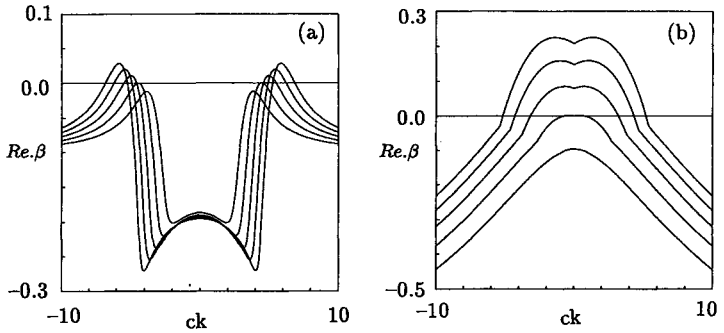


Fig. 1. Real part of linear growth rate Re$\beta$ as a function of $ck=2\pi cq/L$ for various values of $\lambda$; $\lambda=10$, 14, 18, 22 and 26. (a) good cavity case $\kappa=0.1$. (b) bad cavity case $\kappa=5.0$. Here $\gamma_1=\gamma_2=1.0$.

threshold. We show in Figs. 1(a) and (b) how the largest real part of the root $\beta_q$ of Eq. (2·12a) behaves in the good cavity limit (Fig. 1(a)) and in the bad cavity limit (Fig. 1(b)). In the good cavity limit the mode $q=0$ is always stable, and the unstable band, that is, the regions of $q$ in which $\mathrm{Re}(\beta_q)>0$, is localized around the mode number $\pm K_R$, even though the pumping parameter is increased far beyond the threshold of the resonant Rabi instability. Under the bad cavity condition (Fig. 1(b)), on the other hand, even the $q=0$ mode may become unstable (the Lorenz instability), and when the pumping power is slightly increased beyond the instability threshold, the two unstable bands localized around $\pm K_R$ and separated by the $q=0$ mode immediately get broadened and merge into a wide single band covering $q=0$.

### 2.3. *Turbulent states*

We roughly describe here the dynamical states observed beyond the resonant Rabi instability. We show in Figs. 2(a)~(c), the temporal wave forms of electric field intensity $|E(t, z)|^2$ observed at a fixed position together with the energy spectrum of electric field modes $|E(t, q)|^2$ averaged over a long time scale. In the present case we start with the resonant SSS, but the scenario mentioned below is similar even if we

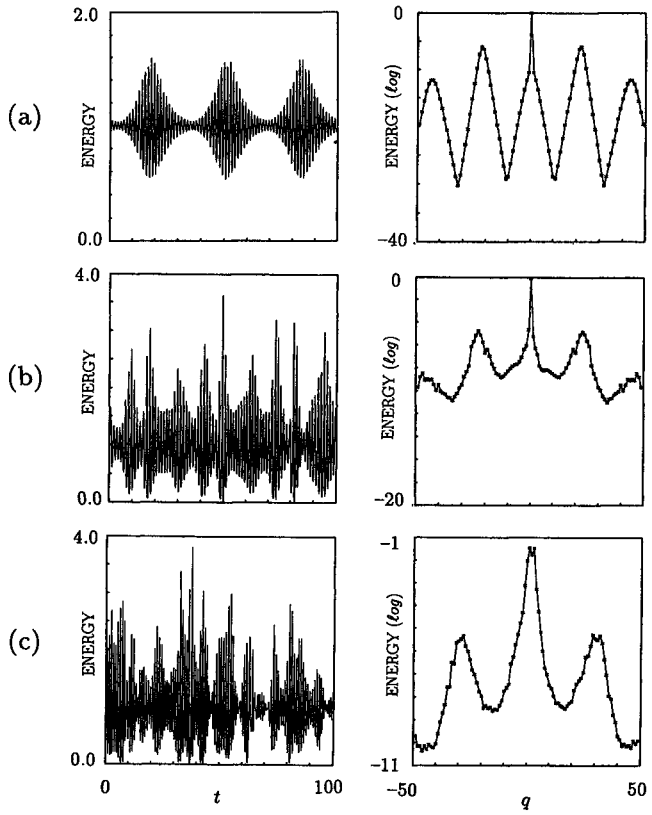


Fig. 2. Wave forms (left) and energy spectra (right) of typical dynamical states above the first threshold. (a) self-locked state ($\lambda=15.5$), (b) localized chaos ($\lambda=18.0$) and (c) global chaos ($\lambda=33.0$). Here $\kappa=.1$, $\gamma_1=\gamma_2=1$, $c=.2125$ and $L=2\pi$.

start with nonresonant SSS.

Immediately after the resonant Rabi instability the SSS becomes unstable and a periodic oscillation with the Rabi frequency takes place, and its amplitude increases in proportion to $\sqrt{(\lambda-\lambda_{\rm th})}$. This is a normal characteristic of the supercritical Hopf bifurcation. With a very slight increase in $\lambda$, the simple sinusoidal oscillation makes a transition to a beating quasi-periodic oscillation ((a)) with two frequencies, i.e., the Rabi frequency and the round trip frequency$=2\pi c_g/L$, where $c_g$ is the group velocity $c_g=(d\mathrm{Im}(\beta_q)/dq)_{q=K_R}$. The latter frequency is much less than the former, and the output forms a pulse train with the period equal to the round trip time $L/c_g$ determined from the mode spacing $d\mathrm{Im}(\beta_q)/dq$ at the unstable mode number $q=K_R$. Such a pulse train is very similar to the one emitted from the mode-locked laser.*) Thus a self-locked laser is self-organized in the Rabi unstable bands. However, the parameter domain in which such an oscillation is observed is not very wide, and as $\lambda$ increases the quasiperiodic oscillation undergoes a transition to a chaotic one as is shown in (b). Up to this stage the time dependent component is small enough and the motion is localized around the SSS with which we started. Such a small amplitude time dependent phenomenon will be described by a simpler model equation such as the complex TDGL model to which the original M-B equation is reduced by using the center manifold perturbation theory. However, we are not interested in such a reduction problem here.

With further increase in $\lambda$, the characteristics of chaotic state drastically changes above a certain threshold (we call hereafter 'the third threshold') and a chaotic state with a quite complex spatio-temporal structure appears ((c)). A remarkable characteristic of this state is reflected in the energy spectrum. Below the third threshold, energy is monopolized by the single mode of the SSS with which we started (the mode $q=0$ in the present case), but above the threshold the energy is distributed over other near resonant modes. We may conjecture that in such a state the motion in the phase space, which has been bounded in the vicinity of the SSS below the third threshold, is released from the restraint of a specific mode and becomes capable of wandering globally over the 'ruins' of other SSSs. It is such a chaotic state that we would like to clarify in the present paper. We point out that a transition to a similar multi-mode oscillating state has been observed for the passive resonator system which exhibits the delay induced instability.[9]

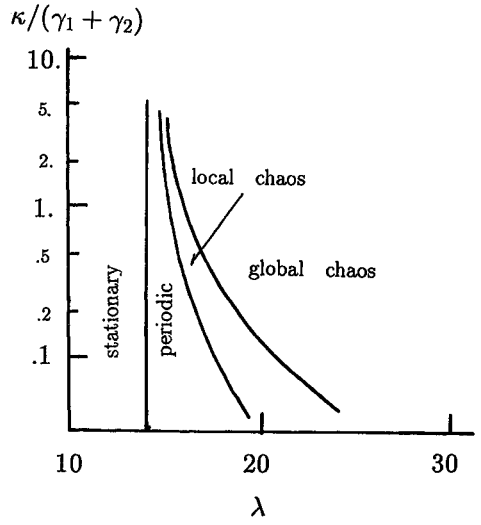


Fig. 3. A rough sketch of the phase diagram of various dynamical states.

*) A similar form of pulse solution has been obtained with a few number of modes analysis. See the paper by Lugiato et al. in Ref. 18).

A rough sketch of the phase diagram of various dynamical states mentioned above are displayed in Fig. 3. Here, we consider the space of the two control parameters $\kappa/(\gamma_1+\gamma_2)$ and $\lambda$. Besides these parameters, our system has two additional control parameters $x=\gamma_1/\gamma_2$ and $L$, but the latter parameter is less relevant for the global structure of phase diagram in the asymptotic limit of $L\to\infty$. In the present paper we consider the specific case $x=1$ although the condition $x\ll 1$ is more realistic in a number of lasers. Under the condition $x=1$ the frequency domain contributing to Rabi oscillation at frequency $\gamma_2\sqrt{\lambda x}$ is well separated from the resonant region ($q\approx 0$) having the width $\gamma_2$, and the analysis becomes rather simpler. In the present paper we further confine ourselves to the good cavity limit and fully investigate the complex dynamical behaviors of the multi-mode oscillation.

## § 3. Information theoretical study of turbulent state

How can we characterize the dynamical structure of the turbulent state of the M-B equation to which a number of degrees of freedom contribute? As is discussed in § 2, the instability which leads eventually to the turbulent behaviour occurs in a restricted region of the wave-number space. Therefore, we may expect that the region in which the chaotic disturbances are generated will be restricted in the wave-number space even in the turbulent state. In order to specify the active region in which chaotic disturbances are generated, we have to quantify how disturbances propagate in the wave-number space and influence the dynamics at different regions in the wave-number space. For this purpose the information theoretical analysis provides a powerful tool.[12),23)] In view of an experimental applicability, this method is useful in particular for optical systems, because the Fourier analyzed time-dependent data can be easily obtained by the spectral analysis of the output. In what follows we show how the information theoretical method enables us to understand the dynamical connectivity formed in the wave-number space.

### 3.1. *Information theoretical quantities*

In order to quantify the amount of connectivity between two dynamical phenomena occurring at two positions, $q_s$ and $q_r$, in the wave-number space, we suppose that there is an information channel between $q_s$(the sender's position) and $q_r$ (the receiver's position) and measure the amount of information exchanged through the channel. The exchanged information is the mutual information shared in common by the two time series of a suitable physical quantity $\epsilon(t, q)$ at $q=q_s$ and $q=q_r$. According to Shannon,[24)] the mutual information (MI) is computed in the following way. First discretize the time series $\epsilon(t, q)$ with an appropriate time interval $\Delta$ as $\epsilon_q(1)$, $\epsilon_q(2)$, $\epsilon_q(3)$, $\cdots$, where $\epsilon_q(k)=\epsilon(k\Delta+T, q)$ and $T$ indicates the origin of the stationary time series arbitrarily chosen. Further, we quantize the variable ranges of $\epsilon(t, q)$ into $N$ finite levels $\alpha_{q_1}, \alpha_{q_2}, \cdots, \alpha_{q_N}$. Then the state of $\epsilon(t, q)$ observed during a time interval $T<t\leq T+j\Delta$ is represented by a string of the $j$ symbols such as $\{\alpha_{q_6}, \alpha_{q_2}, \alpha_{q_6}, \cdots, \alpha_{q_1}\}$, etc. For brevity we denote the statistical event represented by the series $\epsilon_q(1)$, $\epsilon_q(2)$, $\cdots$, $\epsilon_q(j)$ by $E_q^{(j)}$. Then we have $N^j$ possible strings (states) taken by $E_q^{(j)}$. We denote each member of the string by $\alpha_l (1\leq l\leq N^j)$. For each $\alpha_l$ we can compute the

probability of finding it by observing the stationary time series $\epsilon(t, q)$ at various origins $T$. Let $P(\alpha_l)$ be the probability of finding a string $\alpha_l$, then the $j$-steps information $H(E_q^{(j)})$ is defined by

$$H(E_q^{(j)}) = -\sum_l P(\alpha_l)\log(P(\alpha_l)) . \tag{3·1}$$

This quantity characterizes the exponential growth rate of the number of 'sentences' made up by combining the $N^j$ possible 'words'. Hereafter, we omit the superscript $(j)$, if unnecessary.

Next we consider the combined set of the two processes $\epsilon(t, q_s)$ and $\epsilon(t, q_r)$. Let us observe the time sequence $\epsilon(t, q_s)$ and the shifted sequence $\epsilon(t+t_r, q_r)$ for the time interval $T < t \leq T + j\Delta$, where $t_r$ is taken to be an integer multiple of $\Delta$, and let $P(\alpha_l, \beta_m\ t_r)$ be the joint probability of finding the two time series in the combined state $(\alpha_l, \beta_m)$. Then the $j$-steps information carried by the sequences $\epsilon(t, q_s)$ and $\epsilon(t+t_r, q_r)$ (for $T < t \leq T + j\Delta$) is given by

$$\begin{aligned} H(E_{q_s}, E_{q_r}\ t_r) &= -\sum_{lm} P(\alpha_l, \beta_m\ t_r)\log(P(\alpha_l, \beta_m\ t_r)) \\ &= H(E_{q_r}\ t_r, E_{q_s}) , \end{aligned} \tag{3·2}$$

where by the notation "$E_{q_r}\ t_r$" we mean that the event $E_{q_r}$ precedes in time by $t_r$. Let $P(\beta_m\ t_r/\alpha_l)$ be the conditional probability of finding $E_{q_r}(T + t_r < t \leq T + j\Delta + t_r)$ to be in the state $\beta_m$ under the condition of $E_{q_s}$ $(T < t \leq T + j\Delta)$ being in the state $\alpha_l$, i.e.,

$$P(\beta_m\ t_r/\alpha_l) = P(\alpha_q, \beta_m\ t_r)/P(\alpha_l) . \tag{3·3}$$

If we know that the $E_{q_s}$ is in the state $\alpha_l$ then information carried by $E_{q_r}$ is given by $-\sum_m P(\beta_m\ t_r/\alpha_l)\log(P(\beta_m\ t_r/\alpha_l))$ and hence the average amount of the information carried by $E_{q_r}$ alone is

$$\begin{aligned} H(E_{q_r}\ t_r/E_{q_s}) &= -\sum_{lm} P(\alpha_l)P(\beta_m\ t_r/\alpha_l)\log(P(\beta_m\ t_r/\alpha_l)) \\ &= H(E_{q_s}, E_{q_r}\ t_r) - H(E_{q_s}) . \end{aligned} \tag{3·4}$$

Therefore, the information carried in common by the sequences $\epsilon(t, q_s)$ and $\epsilon(t+t_r, q_r)$ (for $T < t \leq T + j\Delta$) is

$$\begin{aligned} I(E_{q_r}\ t_r : E_{q_s}) &= H(E_{q_r}\ t_r) - H(E_{q_r}\ t_r/E_{q_s}) \\ &= H(E_{q_r}) + H(E_{q_s}) - H(E_{q_s}, E_{q_r}\ t_r) \\ &= I(E_{q_s} - t_r : E_{q_r}) \geq 0 , \end{aligned} \tag{3·5}$$

which defines the MI. A remarkable characteristics of the mutual information is that it is semipositive and is zero if and only if the two events $E_{q_s}$ and $E_{q_r}\ t_r$ are statistically independent. The relations among various information theoretical quantities such as $H(E_{q_s}, E_{q_r}\ t_r)$, $H(E_{q_r}\ t_r/E_{q_s})$, $H(E_{q_s})$ and $I(E_{q_r}\ t_r : E_{q_s})$ are intuitively understood in terms of Benn's diagram as illustrated in Fig. 4(a).

According to the similar procedures we can introduce higher order MIs.[23] The 3-point mutual information is of particular importance; it being defined as the infor-

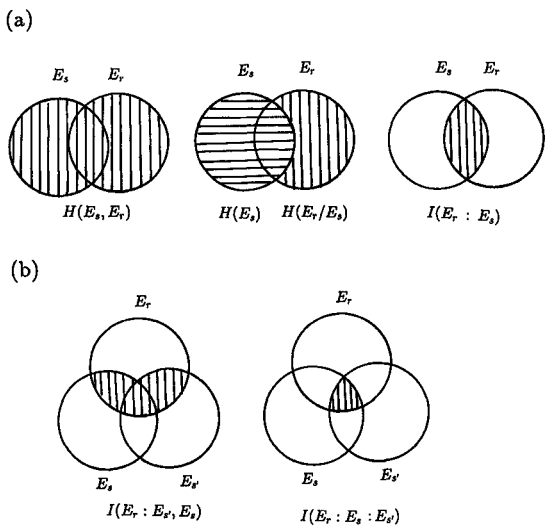


Fig. 4. Relationships among various information theoretical quantities illustrated by Benn's diagram: (a) Quantities related to two events and (b) to three events.

mation shared in common by the time series $\epsilon(t, q_s)$, $\epsilon(t+t_{s'}, q_{s'})$ and $\epsilon(t+t_r, q_r)$ observed for the time interval $T<t \leq T+j\Delta$ at the three different points $q_s$, $q_{s'}$ and $q_r$. Let us denote the combined event composed of $E_{q_{s'}}\, t_{s'}$ and $E_{q_s}$ by $(E_{q_{s'}}\, t_{s'}, E_{q_s})$. Then the MI shared in common with by the combined event $(E_{q_{s'}}\, t_{s'}, E_{q_s})$ and the event $(E_{q_r}\, t_r)$ must be represented by $I(E_{q_r}\, t_r : E_{q's}\, t_{s'}, E_{q_s})$. Then the 3-point MI shared in common by the three events $(E_{q_r}\, t_r)$, $(E_{q_{s'}}\, t_{s'})$ and $E_{q_s}$ should be defined by

$$\begin{aligned} I(E_{q_r}\, t_r : E_{q_{s'}}\, t_{s'} : E_{q_s}) &= I(E_{q_r}\, t_r : E_{q_s}) \\ &\quad + I(E_{q_r}\, t_r : E_{q_{s'}}\, t_{s'}) \\ &\quad - I(E_r\, t_r : E_{q_{s'}}\, t_{s'}, E_{q_s}), \end{aligned} \tag{3·6}$$

where $I(E_r\, t_r : E_{q_{s'}}\, t_{s'})$ may be written as $I(E_r\, t_r - t_{s'} : E_{q_{s'}})$ because of the stationariness. The above relation is easily understood with Benn's diagram depicted in Fig. 4(b). Unlike the 2-point MI, the 3-point MI can be negative, and it has a particularly important significance when it is negative: Suppose a channel with two terminals through which the signals $E_{q_s}$ and $E_{q_{s'}}$ are input. The signal represented by $E_{q_r}$ is output from another terminal. Then we can interpret that the negative 3-point MI, i.e., $\{-I(E_{q_r}\, t_r : E_{q_{s'}}\, t_{s'} : E_{q_s})\}$, which is now positive, measures the amount of MI through the channel which is not included in the 2-point MIs. Indeed Eq. (3·6) is rewritten as

$$-I(E_{q_r}\, t_r : E_{q_{s'}}\, t_{s'} : E_{q_s}) = I(E_r\, t_r : E_{q_{s'}}\, t_{s'}, E_{q_s}) - I(E_{q_r}\, t_r : E_{q_s}) - I(E_{q_r}\, t_r : E_{q's}\, t_{s'}). \tag{3·6'}$$

In other words, the r.h.s. measures the increment of correlation by extending the sender's space so as to include the 'additional' source $E_{q_{s'}}$. As a typical example, let us consider the channel through which two random binary processes, say $X=\{-1, 1\}$ and $Y=\{-1, 1\}$ which are statistically independent, are combined to give the output $Z$ according to the deterministic rule $Z=XY$. As far as the channel $X \to Z$ is concerned, no correlation exists between $X$ and $Z$ and thus no information propagates, i.e., $I(X : Z)=0$ although the output is related to the inputs via a deterministic rule. However, we immediately see that the 3-point MI $I(X : Y : Z)$ has a negative definite value. Existence of the negative 3-point MI is a direct reflection that the apparent absence of correlation between $X$ and $Z$ is due to the modulation by an 'additional' (or 'hidden') process $Y$. It is expected that the 3-point MI is of fundamental importance particularly for the analysis of the systems dominated by 3-wave interaction processes. The M-B system and Navier-Stokes equation are typical

examples of such a class of system.

### 3.2. *Mutual information (MI) map*

*2-point MI map*

In the present analysis we are concerned with how the dynamical fluctuations accompanying the energy (=photon number) of cavity mode propagates in the wave-number space. We, therefore, choose $\epsilon(t, q)$ to be the averaged energy over a finite band

$$\epsilon(t, q)=\sum_{q'=q-dq/2}^{q+dq/2}|E(t, q')|^2/dq\,, \tag{3·7}$$

where $dq$ is the band width appropriately chosen. The result is insensitive to the choice of $dq$ as long as it is small enough. Practically we choose $dq=4$ (sometimes $dq=2$). Further, the computation of MI is carried out, taking the number of quantization levels $N$ to be 2(sometimes 4) and the number of the steps $j$ to be 1. It is convenient to display the mutual information $I(E_{q_r}\, t_r : E_{q_s})$ with a fixed $q_s$ in the form of the contour map on the two dimensional plane of the receiver's time-space $(t_r, q_r)$. We call such a map the MI map. Two typical examples of the MI map are shown in Figs. 5(a) and (b). First we explain how we can read out the dynamical structure from the MI map by using these two examples.

In the case of (a), significant peaks of the MI arrange almost along the line $t_r=0$ with an equal interval. The highest peak is located at $(t_r, q_r)=(0, q_s)$ (this position is indicated by ●) and the temporal decay rate of MI along the line $q_r=q_s$ (we often call $I(E_{q_r=q_s}\, t_r : E_{q_s})$ the self-mutual information) characterizes the *information generating rate* at the sender's position $q_s$. A remarkable fact is that the time at which the MI becomes maximum along a fixed $q_r$ is all delayed from the one at $q_r=q_s$. This fact implies that the disturbances generated at $q_s$ propagate to other regions by skipping processes (indicated by ⟶) or cascading processes (indicated by ⇢).

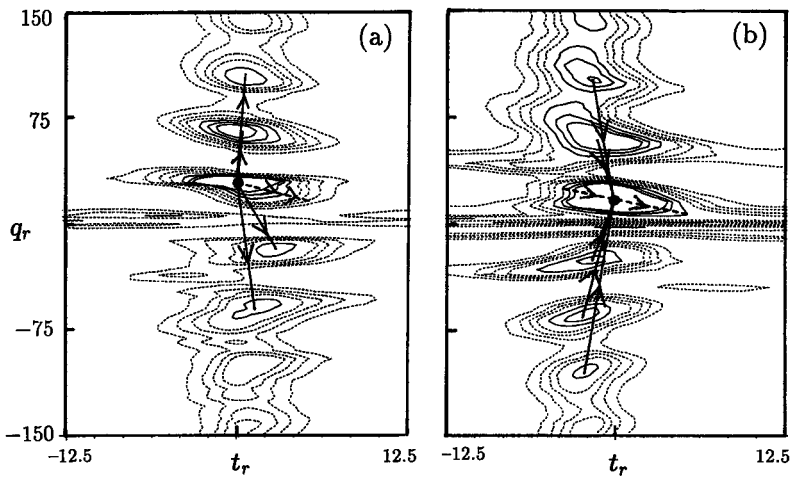


Fig. 5. Two typical examples of 2-point MI map $I(E_{q_r}\, t_r : E_{q_s})$. Here ● indicates the sender's time and position. $\kappa=.5$, $\lambda=30.$, $\gamma_1=\gamma_2=1.$, $c=.1517$ and $L=2\pi$.

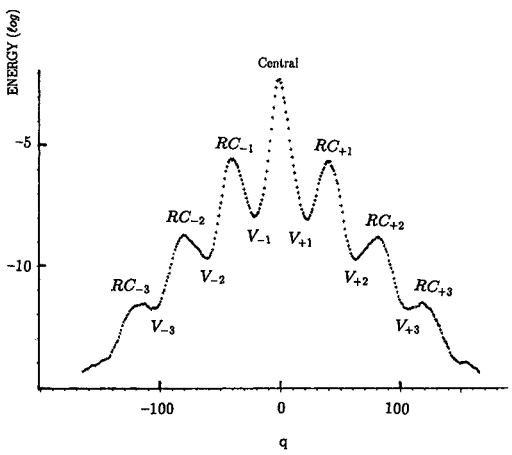


Fig. 6. Energy spectrum and locations of various regions (see the text) in the wave-number space. Parameters are the same as in Fig. 5.

Thus Fig. 5(a) provides a typical example when $q_s$ is a source of generating disturbances. On the other hand, (b) presents a sharp contrast to (a): the sender's position $q_s$ receives the disturbance from the higher wave-number side and propagates it toward the lower wave-number side by a cascading process. Moreover, it is influenced via skipping processes from all other regions with significant peaks of MI. Hence it is unlikely that any significant disturbances are generated here.

According to the way explained above, we can read out from the MI map how information carried by the disturbances is generated and propagates in the wave-number space. We show in Figs. 7(a) ~(g) a series of the MI maps computed for several representative positions of $q_s$. Comparing the information structures read out from them, we can obtain a global picture of the information network formed in the wave-number space. In particular it is possible to specify the source region in which chaotic disturbances are generated.

Before describing the information structure of the turbulent state, we show in Fig. 6 the energy spectrum (this may be identified with the photon number spectrum) in the wave-number space. The highest peak is located at the resonance $q=0$, and most of the radiation energy is concentrated there. We call the region in the vicinity of $q=0$ the *central range*. Besides the peak at $q=0$, other noticeable peaks are located near at the wave numbers of the resonant Rabi instability, i.e., $\pm K_R(K_R=k_R/(2\pi/L)$; see Eq. (2·14) and at its higher harmonics $\pm 2K_R$, $\pm 3K_R$, etc. We denote the energetically rich regions surrounding these peak positions by $RC_{\pm 1}$, $RC_{\pm 2}$, $RC_{\pm 3}$, etc. On the other hand, the energetically poor regions surrounding the centers of the two peak positions are denoted by $V_{\pm 1}$, $V_{\pm 2}$, etc. The positions of $q_s$ in (a)~(g) of Fig. 7 are so chosen as to represent these regions, namely

| | | | |
|---|---|---|---|
| (a) | represents | central range | ($q_s=0$) |
| (b) | | $V_{+1}$ | ($q_s=15$) |
| (c)(d)(e) | | $RC_{+1}$ | ($q_s=30, 39, 45$) |
| (f) | | $V_{+2}$ | ($q_s=66$) |
| (g) | | $RC_{+2}$ | ($q_s=84$). |

The regions $RC_{+1}$ and $RC_{-1}$ are called the Rabi chaotic bands since, as will be shown below, the chaotic disturbances are generated there. $RC_{\pm 1}$ split further into two regions, i.e., the upper band ($RC_{\pm U}$) and the lower band ($RC_{\pm L}$) belonging to different information networks, and

| | | |
|---|---|---|
| (c)(d) | represent | $RC_{+L}$ |
| (e) | | $RC_{+U}$. |

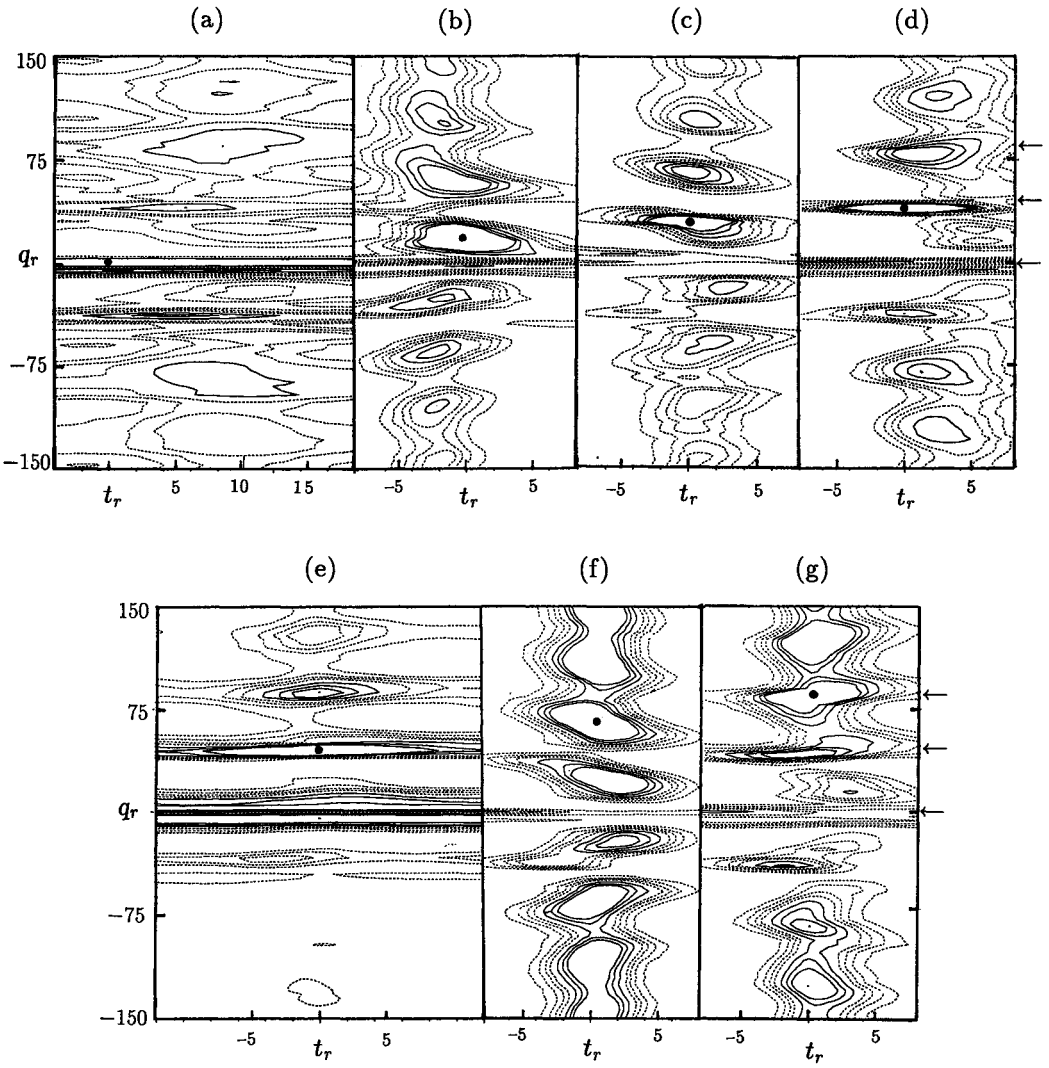


Fig. 7. 2-point MI maps for various sender's positions (indicated by ●), i.e., (a) $q_s=0$, (b) $q_s=15$, (c) $q_s=30$, (d) $q_s=39$, (e) $q_s=45$, (f) $q_s=66$ and (g) $q_s=84$. The central range ($q=0$), $RC_{+1}$ and $RC_{+2}$ are indicated by ←. Levels of contour lines are ···0.005(bit), ···0.010, ···0.015, ···0.020, —0.030, —0.040 and —0.050. Parameters are the same as in Fig. 5. See the text for the correspondence between each $q_s$ of (a)~(g) and each of the regions illustrated in Fig. 6.

Now let us observe the MI maps shown in Figs. 7(a)~(g). From each of the MI map we can read out that the following connections are formed in the wave-number space:

(a) $q_s \rightarrow RC_{+1}$ and $RC_{+2}$ and $RC_{-1}$ and $RC_{-2}$,

(b) $RC_{+L} \rightarrow$ ⓒ$q_s \rightarrow$ ⓒ lower wave numbers;

$V_{+2}$ and $V_{+3} \rightarrow q_s$; $RC_{-L}[-K_R+q_s] \rightarrow q_s$; $V_{-2} \rightarrow q_s$,

(c) $q_s \rightarrow$ ⓒ $V_{+1}$ ; $q_s \rightarrow V_{+2}[2q_s]$ ; $q_s \rightarrow V_{+3}[3q_s$ or $2q_s+K_R]$ and $V_{-1}[-2q_s]$,

(d) $q_s \rightarrow V_{+2}[2q_s]$ ; $q_s \rightarrow V_{+3}[3q_s]$ and $V_{-2}[-2q_s]$,

(e) central range $\rightarrow q_s$ ; $q_s \rightarrow RC_{+2}[2q_s]$ ; $q_s \rightarrow RC_{+3}[3q_s]$,

(f) $RC_{+L} \rightarrow q_s \rightarrow V_{+1}$ ; $q_s = V_{-2}$ and higher wave number beyond $V_{+3}[q_s+K_R]$ and $V_{-3}$ ; $q_s \rightarrow V_{-1}$,

(g) $RC_{+U}[K_R] \rightarrow q_s$ ; $q_s = RC_{-2}$ and higher wave number beyond $RC_{\pm 3}[\pm 3K_R]$ ; $RC_{-U}[-K_R] \rightarrow q_s$.

Processes are arranged in order of decreasing correlation. Here, the notation $X = Y$ means that the two regions $X$ and $Y$ are correlated simultaneously and neither of the two precedes the other one, and the symbol ⓒ indicates the cascade process. By the notation $X[q_x]$ we show the wave number $(q_x)$ representing the region $X$. Taking into account the main processes alone, we see that the two main networks as follows are formed in the wave-number space:

$$\text{central range} \rightarrow RC_{\pm U} \rightarrow RC_{\pm 2} = \text{higher wave-number region}$$

$$RC_{\pm L} \rightarrow V_{\pm 2} = \text{higher wave-number region}$$

$$\searrow \text{ⓒ } V_{\pm 1}.$$

At first glance the central range seems to be a source of chaotic disturbance. However, as is seen from Fig. 7(a), the decay rate of the self-mutual information along the line $q_r = q_s$ is quite small. This fact means that the dynamics in the central range surely controls the $RC_{\pm U}$ but its time scale is considerably long (time scale=100-200) and its dynamics is irrelevant to the downstream processes originating from $RC_{\pm U}$ which have much shorter time scale (time scale=5-10; see the dacay rate of the self-mutual information of Figs. 7(c)~(e)). However, the correlation between the central range and the Rabi chaotic band is quite important. The physical significances of the long time scale characterizing the central range and of the interplay between the central range and the Rabi band are discussed in detail in § 4. Thus the turbulent disturbances are generated in $RC_{\pm U}$ and $RC_{\pm L}$, i.e., in the Rabi chaotic bands.

The distribution of MI is in general localized around the highest peak at $(q_r, t_r) = (q_s, 0)$ (indicated by ●). Let $D(q_s)$ be the localization width of MI measured in the wave-number space around $q_r = q_s$. A striking feature of the MI with $q_s$ in the Rabi chaotic band is that the width $D(q_s)$ is quite narrow (see the localized structures of the MI around ● in Figs. 7(c)~(e)) and is as large as the band width $dq$ of the averaging procedure (see Eq. (3·7)). Therefore, we may conjecture that chaotic disturbances are generated almost independently by all the modes in the Rabi chaotic bands, and we can evaluate the dimension of attractor by the number of modes contained in $RC_{\pm 1}$. Thus the region $RC_{\pm 1}$ correspond to the *attractor interior*.

In contrast to the Rabi chaotic bands, the higher wave-number regions beyond the

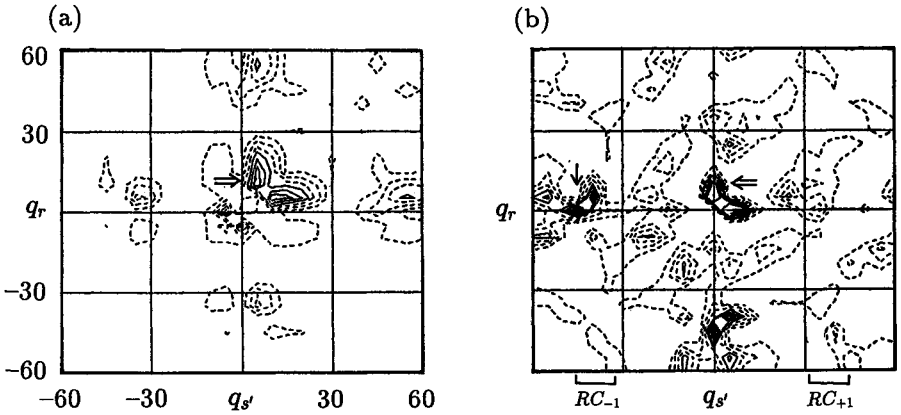


Fig. 8. 3-point MI contour maps for the sender's position taken (a) in $RC_{+L}(q_s=30)$ and (b) in $RC_{+U}(q_s=45)$. For details see the text. Levels of contour lines are ⋯; −0.001(bit), ⋯; −0.002, ⋯; −0.003, —; −0.004, —; −0.005⋯. Parameters are the same as in Fig. 5.

regions $V_{\pm 2}$ and $RC_{\pm 1}$ are strongly correlated without any time delay (Figs. 7(f), (g)). This is a common property of the *attractor exterior* which has been observed in other systems as well.[12] The typical regions corresponding to the *attractor exterior* is $V_{\pm 1}$, $V_{\pm 2}$, $RC_{\pm 2}$, $RC_{\pm 3}$, etc. The peaks in the MI map arranged with equal interval is placed almost at the position $q_r=q_s+$(integer multiple of $K_R$), which must be due to the 3-wave interaction process such as $q_1(=q_s)+q_2(=K_R)\rightarrow q_3(q_r)$ inherent in the M-B system (see Eq. (2·1′a∼c)).

*3-point MI map*

Finally we show in Fig. 8 examples of the 3-point MI map at two fixed positions taken in the Rabi chaotic band. As discussed in § 3.1, the negative value of the 3-point MI is of particular importance. We, therefore, compute the maximum value of $\mathrm{Max}(-I(q_r\ t_r : q_{s'}\ t_{s'} : q_s), 0)$ over the two times $t_r$ and $t_{s'}$ and display its contour map on the plane $(q_{s'}, q_r)$. From the definition, the contour plot is symmetric with respect to the line $q_{s'}=q_r$. A noticeable fact is that the 3-point MI does not have appreciable value for $q_r$(or $q_{s'}$) in the Rabi unstable bands $RC_{\pm 1}$. This fact suggests that the strong decorrelation represented by the smallness of the 2-point MI in the Rabi unstable bands can by no means be attributed to a randomization due to a hidden variable at any $q_{s'}$. This provides a further evidence that the absence of correlation among the motions in the Rabi chaotic bands is not apparent and these motions are intrinsically independent of each other.

A further noteworthy facts read out from the 3-point MI map is that it has remarkable peaks at two positions indicated by arrows in Fig. 8. One peak (indicated by →) is situated at $q_r$ and $q_{s'}$ in the central range and in $RC_{-1}$, respectively (and vice versa). This allows us to interpret that the processes such as

$$RC_{+1}+RC_{-1}\rightarrow \text{central}$$

$$RC_{+1}+\text{central}\rightarrow RC_{-1}\,,\quad \text{etc.},$$

are specifically activated. These processes are consistent with the 3-wave interaction which conserves the wave number, and they provide further evidences showing the presence of a strongly correlated motion among the two Rabi chaotic bands and the central range. Further, a study of the time dependent 3-point MI map reveals more clearly that the Rabi chaotic bands have two time scales; the shorter time scale characterizing the generation of chaotic disturbances and the longer time scale due to the motion correlated with the central range. The physical phenomena associated with the correlated process will be discussed in detail in the next section.

On the other hand, the process implied by the other peak (indicated by $\Rightarrow$) is not easy to interpret. In fact the meaning of the $q_r$ of the peak position cannot be identified, while the $q_{s'}$ is evidently in the central range. $q_r$ seems to be at the position of a fractional harmonic of $RC_{+1}$. Possibility of the fractional harmonic instability in the wave-number domain has been reported in a Dye laser experiment by Hillman et al.[26] They reported that above the first threshold subcritical transitions to the 1/2 harmonic and further to 1/3 harmonic take place successively. Such a drastic transitions have not been reproduced at all in the present study of the M-B model, however, the above result of the 3-points MI map may imply that the turbulent state has a potential for generating fractional harmonics although the processes are negligible from an energetic point of view. Thus the MI method enables detecting dynamical processes which are very difficult to detect by usual spectroscopic methods based upon static measurement of energy spectrum.[25]

## § 4. Chaotic itinerancy : dynamics in the central range

More than 90% of the total energy is distributed to the central range. In the present section we show that in the turbulent state the central modes exhibit two remarkable dynamical phenomena which have been often observed in multi-mode laser oscillations. These phenomena have been so far understood in terms of photon number dynamics modulated by *externally* applied random noise. In the M-B system, however, the origin of such phenomena is chaos generated by the system *itself* and moreover a topological constraint inherent in the M-B system plays an essential role.

### 4.1. *Shorter time scale: self-induced mode partition noise*

*Simple topology of the slow manifold*

The 2-point and the 3-point MI map suggest that the nonlinear coupling between the two Rabi chaotic bands much influences the dynamics of the central range. To examine the effect of the Rabi chaotic bands, we observe what occurs when one of the two Rabi bands is 'removed' from the original M-B system. The removal is achieved by making the amplitudes of all the modes in one of the two Rabi bands zero at each step of numerical integration. Chaotic variation of the central modes ceases after the removing operation, and though the modes scramble for energy for a while, a single mode stationary solution (SSS) is eventually realized. Hence the M-B system is stabilized without one of the two Rabi chaotic bands. A remarkable feature of the 'stabilized M-B system' is that it exhibits a mode competition in which one of the

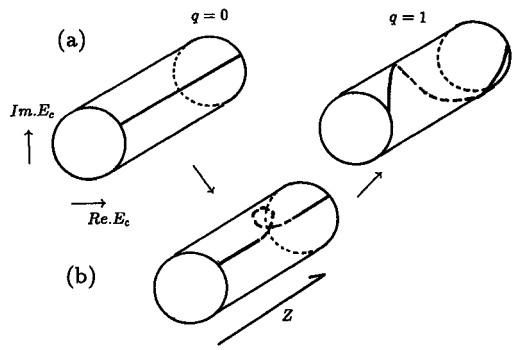


Fig. 9. (a) Spatial configurations of $E(t, z)$ corresponding to the single mode stationary solutions (SSS) with the $q=0$ and $q=1$, and (b) typical configuration which appears in the halfway through the transition from the $q=0$ to $q=1$. A 'loop structure' is nucleated.

modes suppresses all other modes. What mode finally survives the competition depends not on the initial distribution of photon numbers over the central modes but on the topological characteristic possessed by the initial configuration. Now let us discuss briefly a simple topological property inherent in the stabilized M-B system.

Suppose that there is no spatial coupling in the original M-B equations (2·1 a~c), i.e., $c=0$. Then it becomes an assembly of uncoupled single mode laser rate equation (=Lorenz equation), each of which is stable under the good cavity condition considered here. Therefore, the state of the system rapidly relaxes to the stationary lasing state with $|E(t, z)|=|P(t, z)|=1$, where the relative phase of $E(t, z)$ to $P(t, z)$ becomes fixed. In other words, the spatial configuration of the complex field amplitude started with arbitrary configuration relaxes onto the torus defined by $|E(t, z)|=1(0\leq z\leq L)$. Without the spatial coupling, the absolute phase $\phi(t, z)$ of $E(t, z)$ at any spatial positions can be chosen arbitrarily. However, once the spatial coupling due to the propagation effect is introduced, the stable spatial configuration of phase is automatically selected. The family of the single mode stationary states defined by Eqs. (2·5a~c) corresponds to such stable configurations. Quite important fact to be noted is that the single mode stationary states have different topological characteristics; each of them being specified by the winding number defined by

$$\tilde{W}(t)=(\phi(t, z=L)-\phi(t, z=0))/2\pi\,. \tag{4·1}$$

The resonant state with $q=0$ has the winding number 0, and the off resonant state with $q=1$ the winding number 1 and so on (see Fig. 9(a)). As far as the coupling strength is not very strong, it is easy to deform the spatial configuration of phase $|E(t, z)|=1(0\leq z\leq L)$ with a given winding number on the torus, in other words, it takes a long time in relation to the coupling strength for a deformed configuration to relax to the configuration of the single mode stationary solution. Thus the torus $|E(t, z)|=1(0\leq z\leq L)$ forms a slow manifold on which the spatial configuration of phase varies quite slowly in time. We note that there are a number of slow manifolds characterized by different winding numbers 0., $\pm1$, $\pm2$, ….

It is easy to show that the motion on the slow manifold is described by a diffusion equation for the phase variables: Remember that the linearized motion of the phases of $E(t, z)$ and $P(t, z)$ around the resonant stationary solution exhibits a coupled motion described by the characteristic equation (2·12b), which has a root approaching zero in the limit $q\to0$. The root is expanded in the vicinity of $k=0$ as

$$\beta_q=-ivk-Dk^2+O(k^3)\,, \tag{4·2}$$

where $v=\gamma_2 c/(\gamma_2+\kappa)$, $D=\gamma_2\kappa c^2/(\gamma_2+\kappa)^3$ and $k=2\pi q/L$. This fact means that an appropriate linear combination of $\phi$ and $\psi$ (=phase of $P(t, z)$) denoted by $\Psi$ satisfies the following diffusion equation:

$$\frac{\partial\Psi}{\partial t}+v\frac{\partial\Psi}{\partial z}=D\frac{\partial^2\Psi}{\partial z^2}. \tag{4·3}$$

In order to describe a more general motion on the slow manifolds with the winding numbers $\tilde{W}\neq 0$, we have to take into account the nonlinear term due to the spatial phase derivative. The derivation of the equation is a tedious but straightforward calculation of the center manifold perturbation theory. The result is

$$\frac{\partial\Psi}{\partial t}+v\frac{\partial\Psi}{\partial z}=D\left(\left|\frac{\partial\Psi}{\partial z}\right|^2\right)\frac{\partial^2\Psi}{\partial z^2}+a_3\frac{\partial^3\Psi}{\partial z^3}+a_4\frac{\partial^4\Psi}{\partial z^4}, \tag{4·4}$$

where, $a_3=-\kappa^2\gamma_2 c^3/(\kappa+\gamma_2)^5$, $a_4=\kappa^3\gamma_2 c^4/(\kappa+\gamma_2)^7$, and the amplitude-dependent diffusion constant is defined by $D(|\partial\Psi/\partial z|^2)=\kappa\gamma_2 c^2[1-(\kappa\lambda+\kappa+\gamma_2)c^2|\partial\Psi/\partial z|^2/(\kappa+\gamma_2)^2\kappa\lambda]/(\kappa+\gamma_2)^3$. Equation (4·4) describes the relaxation motion toward the single mode stationary solution on the slow manifold with a small winding number $\tilde{W}\neq 0$. However, we emphasize that the slow manifold with relatively large winding number satisfying $|\tilde{W}|>q_c\sim\gamma_2 L/2\pi c$ is unstable (see Eq. (2·6)).

*Self-induced mode partition noise*

The actual motion of the modes in the central range is significantly perturbed by the nonlinear coupling between the two Rabi bands. We show in Fig. 10 how the photon numbers (or energy) of the central modes vary in time in the turbulent state discussed so far. For comparison we plot the total photon number distributed to the central modes. Although the total photon number does not appreciably fluctuate around the mean value, the photon number of each mode fluctuates quite violently. This fact means that photon numbers tend to be repartitioned actively among the central modes under the restriction of the total photon number being almost conserved. A quite interesting fact is that such a fluctuation is often observed in experiments of multimode laser oscillation and is called *mode partition noise.*[27] The time scale of the mode partition noise is in general much longer than other time scales of lasing. In fact it characterizes the anomalously long memory of the self-mutual information in the central range displayed in Fig. 7(a). Presence of such a time scale is closely related with the existence of slow manifold discussed in

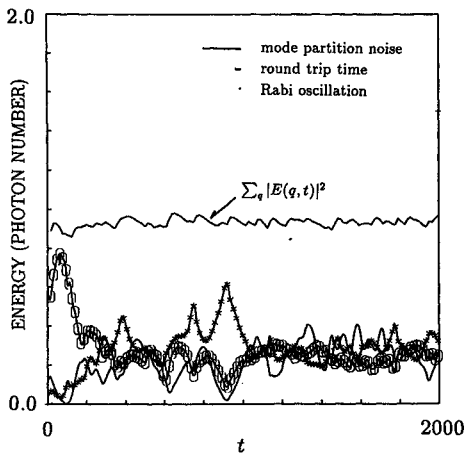


Fig. 10. Mode partition noise: Temporal variation of energy (=photon numbers) of three different central modes and of total energy in the core range. Typical time scales of various dynamical phenomena are also shown. Here, $\lambda=30$, and other parameters are the same as in Fig. 2.

the previous subsection. The mode partition noise has been described by conventional photon number dynamics driven by externally applied random noise.[28] However, the mechanism which originates the mode partition noise is quite different in our system. First the origin is chaos generated by the system itself, and moreover the phase of electric field on the slow manifold plays an essential role.

With a given winding number the spatial configuration of $\phi(t, z)$ moves with the velocity $v$(Eq. (4·3)) and deforms quite slowly in time on the torus $|E(t, z)|=1(0\leq z \leq L)$ under the influence of rapidly varying perturbation from the Rabi chaotic bands. Such a motion necessarily makes the phase derivative spatially nonuniform. Since $\phi(t, z)$ is a slowly varying function of $\xi=z-vt$ (moving frame) and $\tau=t$ viz., $\phi(t, z)=\tilde{\phi}(\tau, \xi)$ and the electric field is given approximately by $E(t, z)=\exp(i\phi(t, z))$, its Fourier component is computed roughly by using the stationary phase approximation as

$$|E(q, t)|\sim|\sum_j(i\partial^2\tilde{\phi}(\tau, \xi_j)/\partial\xi_j^2)^{-1/2}|\,, \tag{4·5a}$$

where $\xi_j$ is the positions satisfying the condition

$$2\pi q/L=\partial\tilde{\phi}(\tau, \xi_j)/\partial\xi_j\,. \tag{4·5b}$$

Thus an appearance of the the spatial nonuniformity in the phase derivative means that modes with wave numbers other than the winding number are excited. Needless to say, the intensity of the total field is almost invariant because $E(t, z)$ is on the torus $|E(t, z)|=1$. This is the origin of the mode partition noise in our system. The time scale of the mode partition noise is easily estimated from the diffusion equation (4·3): let $E_c(t, z)$ be the amplitude of the electric field made up from the mode $E(t, q)$ in the central range, i.e.,

$$E_c(t, z)=\sum_{q\in\text{central range}}E(t, q)e^{i2\pi qz/L}\,, \tag{4·6}$$

and let $\phi_c(t, q)$ be the phase fluctuation mode with the mode number $q$. We suppose that the system is in the state with winding number $\tilde{W}=0$ and the phase fluctuates quite slowly in space. Since $E_c(t, z)=\exp i[\sum_q\phi_c(t, q)e^{i2\pi qz/L}]$, we obtain

$$\delta E_c(t, q)=i\phi_c(t, q)e^{i\phi_c(t, q=0)}\,, \tag{4·7}$$

where $\delta E_c(t, q)$ stands for the $q$-th Fourier component of fluctuation of central field $E_c(t, z)$. Consequently, the inverse of the decay rate of the phase mode which is closest but not equal to zero characterizes the time scale of the central range. From the Fourier transformed version of Eq. (4·3) (or from Eq. (4·2)) we can evaluate the time scale of the mode partition noise:

$$(\mathrm{Re}\beta_{q=1})^{-1}\sim(\gamma_2+\kappa)^3L^2/(4\pi^2\gamma_2c^2\kappa)\,, \tag{4·8}$$

which is very long since it contains the system size $L$. The slow fluctuation in the central range in turn modulates the rapid motion in the Rabi chaotic bands and hence induces a long time scale component of the motion there.

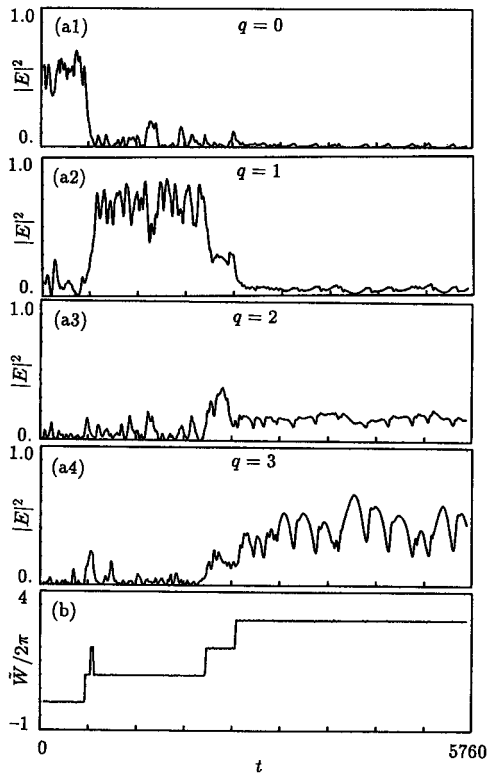


Fig. 11. Mode-hopping: Temporal variations of energy(=photon numbers) of the core modes. (a1) $q=0$, (a2) $q=1$, (a3) $q=2$, (a4) $q=3$, and (b) temporal variation of winding number. Here $\lambda=33$, and other parameters are the same as in Fig. 2.

### 4.2. *Longer time scale: self-induced mode hopping*

*The mode hopping*

On a time scale much longer than that of the mode partition noise a drastic phenomenon is observed in the dynamics of the central range. In Figs. 11(a1) ~(a4) we show a typical example of the temporal variation of photon numbers of the central modes. In this figure the time scale is taken so long that the mode partition noise looks like a rapid fluctuation. A quite remarkable fact is that on such a long time scale the distribution of photon numbers over the central modes often changes drastically. In this example the number of the most predominantly excited mode changes successively as $q=0\rightarrow q=1\rightarrow q=2\rightarrow\cdots$.

Quite similar phenomena described above have been often observed in multi-mode oscillation of lasers such as semiconductor laser, solid state laser and so on, and they have been called mode hopping.[2] In the actual analysis of the mode hopping the rate equation for photon number, which was founded by Lamb et al. in order to describe multi-mode competition,[20] is usually employed: The rate equation has stable fixed points corresponding to the single mode stationary states, and a random and uncontrollable *quantum noise* introduced externally induces the hopping among the stable fixed points (Ohtsu et al.).[29]

However, the underlying mechanism of the mode hopping phenomenon observed in the M-B system is quite different from the one described by the randomly perturbed Lamb's photon number dynamics in which the role of phase is discarded:[20] We note that the mode hopping of the M-B system is closely related with the change of the topological characteristic. We depict in Fig. 11(b) the time evolution of the winding number $\tilde{W}(t)$ associated with the central field $E_c(t, z)$. The mode hopping takes place at the time when the winding number suddenly changes. This fact means that the mode hopping is an itinerant motion over the chaotic attractors each of which grows from a stationary single mode solution (SSS) and is localized around it with a definite winding number. In the former half of time evolution depicted in Fig. 11 photons are monopolized by the single mode with the same mode number as the winding number, but photons can in general be distributed over multiple modes with

the mode number close to the winding number. The number of photons distributed to a mode is almost conserved except for the variation due to the mode partition noise until a mode hopping takes place. Example of such *multi-mode firing states* is seen in the latter half of the time evolution shown in Fig. 11 and in the example depicted in Fig. 10.

It is very easy to deform the spatial configuration of $E(t, z)$ on the slow manifold with a given winding number. Such a deformation results in the mode partition noise. However, it is very hard to make a transition between two slow manifolds with different winding numbers, because in order to deform the spatial configuration of $E(t, z)$ so as to change the winding number the configuration must be removed off from the torus and a 'loop' must be nucleated (see Fig. 9(b)). A quite similar situation is seen in the decay process of persistent current in the superconductor. However, unlike the case of superconductor, the source which causes the transition in our system is not the thermal noise but a deterministic chaos. In what follows we show that a quite ingenious mechanism which makes it much easier to change the topological characteristic is self-generated through the chaotic dynamics of our system.

*Self-formation of easy paths*

Hereafter we show that when a mode hopping is taking place an easy path through which the spatial configuration of the system changes its topological characteristic is self-generated owing to a close interplay between the modes in the central range and the ones in the Rabi chaotic bands. To this end we introduce physical quantities which characterize the dynamics in the central range and the Rabi chaotic bands. The state of the central range is described by the central field $E_c(t, z)$ defined by Eq. (4·6). On the other hand, we have to introduce any quantity characterizing the state of the Rabi chaotic bands. From Eqs. (2·1'a~c) the Fourier component of the 'force' which originates from the Rabi chaotic bands and perturbs the motion of the central mode must be defined as

$$F_P(t, q)=\gamma_2 \sum_{q_1+q_2=q} E(q_1) W(q_2)\,, \tag{4·9a}$$

$$F_W(t, q)=-\frac{\lambda\gamma_1}{2} \sum_{q_1+q_2=q} [E^*(-q_1)P(q_2)+E(q_1)P^*(-q_2)]\,, \tag{4·9b}$$

where either of $q_1$ or $q_2$ ranges in the two Rabi chaotic bands. Therefore,

$$F_{P,W}(t, z)=\sum_q F_{P,W}(t, q)e^{i2\pi qz/L} \tag{4·10}$$

describes the spatial pattern of the perturbation originating from the Rabi chaotic bands. We call these the Rabi forces. We show in Fig. 12 what is happening when the winding number changes from 1 to 2. The series (a)~(c) represent time evolutions of the following quantities, i.e., (a) the spatial trajectory of $E_c(t, z)$, (b) the spatial pattern of the phase $\phi_c(t, z)$ of $E_c(t, z)$, and (c) the spatial pattern of the modulus of the Rabi force, respectively. A remarkable fact to be noted is that the spatial pattern of the Rabi force has remarkable peaks (we call these force peaks), and that the spatial phase pattern, on the other hand, has inflections indicated by arrows (see $t=0$, $t=360$ and $t=760$; called the *phase inflections* from now on). These

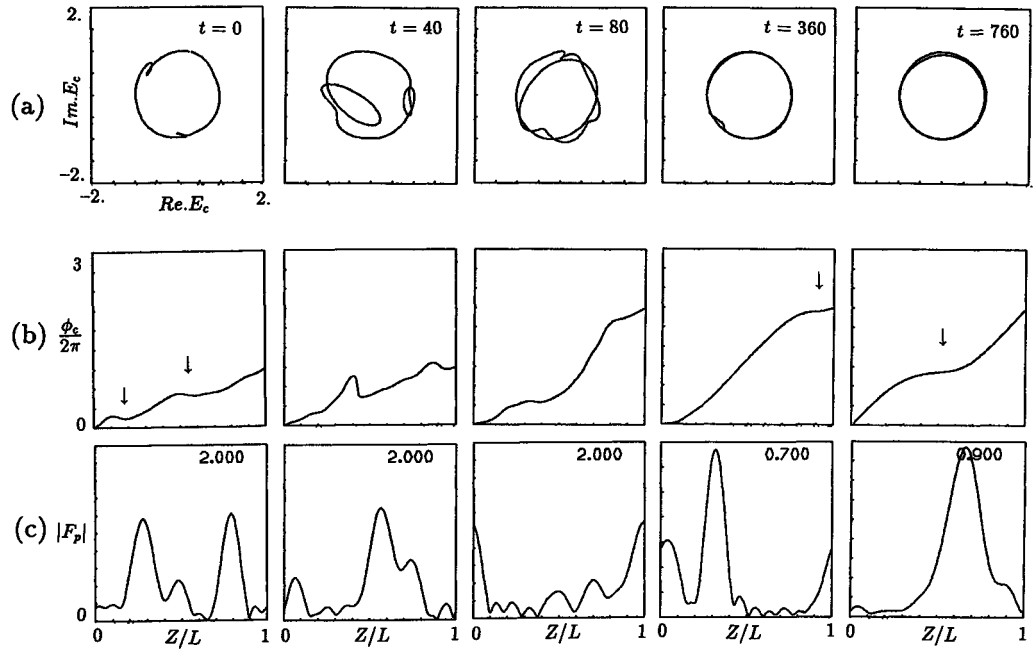


Fig. 12. Temporal evolutions of the spatial trajectory of the complex central field $E_c(t, z)$ (series (a)), of the spatial pattern of the phase $\phi_c(t, z)$ (series (b)), and of the spatial pattern of the Rabi force amplitude $F_P(t, z)$ (series (c)). Transition process through which the winding number changes by $1(t=0\sim80)$, and typical situations in the quasi-stationary state after the transition ($t=360$, $t=760$). The inserted number in (c) stands for the length of the ordinate. Parameters are all the same as in Fig. 10. Typical phase inflections are indicated by ↓.

objects move to right with light velocity and the force peaks go slightly ahead the phase inflections. When the height of a force peak increases, a bulge grows from a phase inflection ($t=40$) to form a "loop" structure, and a transition to a new state with a larger winding number is eventually achieved. Then which of the two phenomena, namely the appearance of phase inflections and the formation of force peaks, is the essential origin of the mode hopping? We examine this problem in the *transplant experiment* described below.

Let us consider two identical M-B systems, systems I and II. We compute the time dependent data of the variables $E(t, q)$, $P(t, q)$ and $W(t, q)$ in a specific wave-number region, say TP, of system I. We 'transplant' the data of I to the same wave-number region of system II and observe the time evolution of system II. The 'transplant operation' represents to replace $E(t, q)$, $P(t, q)$ and $W(t, q)$ in the wave-number region TP of system II by those of system I at each step of numerical integration. By observing the motion of system II, we can immediately examine how the wave-number region other than TP is influenced from the region TP to which the data created by system I through a natural evolution is transplanted.

In the first experiment the data taken at the Rabi chaotic bands are transplanted to the Rabi bands of system II, and the evolution of the central range is observed. As shown in Fig. 13(a) the Rabi chaotic bands form the Rabi force with two noticeable peaks. In the initial stage we excite only the mode $q=1$ in the central range of

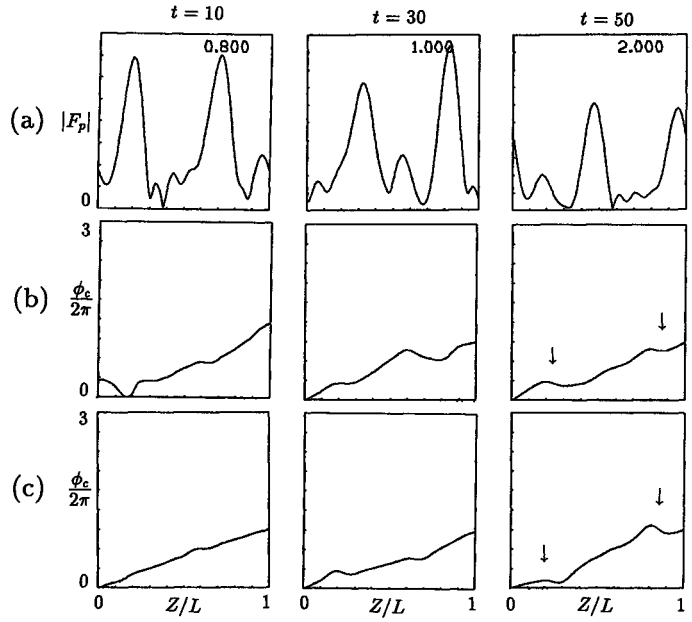


Fig. 13. Transplant experiment 1: (a) Spatial pattern of the Rabi force formed through a natural evolution of the system I. (b) Phase inflections formed through the same evolution process as in (a). (c) Formation of phase inflections in system II by the transplanted Rabi chaotic bands data corresponding to (a).

system II, and hence the central field varies spatially as $E_c(t=0, z)=\exp(2\pi z/L)$ and the spatial pattern of $\phi_c(t=0, z)$ forms a straight line. However, as shown in Fig. 13(c), the spatial phase pattern gets distorted as time elapses. In particular phase inflections quite similar to the ones formed through the natural evolution in system I (Fig. 13(b)) emerge behind the force peaks (Fig. 13(c)), which strongly implies that the Rabi force peaks are the origin of the phase inflections.

The second experiment is a reversed version of the first one: We transplant the data obtained for the central range of system I to that of system II and observe the development of spatial pattern of the Rabi force. In the initial stage the modes in the Rabi chaotic bands are excited at random with very small amplitudes. We show in Figs. 14(c1)~(c3) three examples of the spatial pattern of the Rabi force formed in system II by using the same central range data transplanted, where the initial states of the Rabi bands are different from each other. It is evident that in all examples noticeable peaks are formed slightly ahead from the phase inflections depicted in (a). Moreover, the positions of the force peaks coincide quite well with those due to the natural evolution of system I (see (b)). This fact strongly implies that the force peaks grow adapting themselves to the positions of the phase inflections.

The above two complementary experiments strongly suggest that the interplay between the central range and the Rabi chaotic bands works cooperatively in making the system change its topological characteristic: If a phase inflection is formed in the central field, then the radiation in the Rabi chaotic bands changes so as to enhance the Rabi force at the positions slightly advanced from the positions of the phase inflections, and the enhanced peaks of the Rabi force in turn distort further the phase

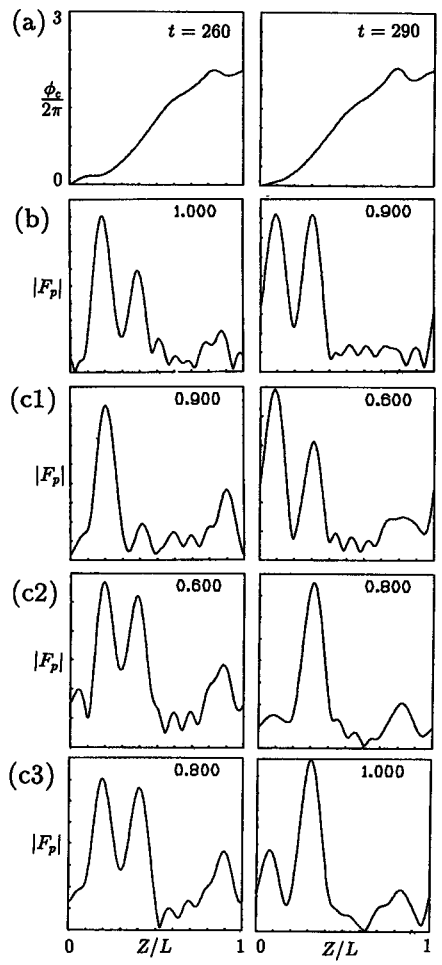


Fig. 14. Transplant experiment 2: (a) Spatial pattern of the phase $\phi_c(t, z)$ formed through a natural evolution of system I. (b) Spatial pattern of the Rabi force formed through the same evolution process as in (a). (c1)~(c3) show the spatial pattern of the Rabi force formed in system II to which the central range data corresponding to (a) is transplanted.

inflections formed in the central field. In other words, the interplay between the Rabi bands and the central range induces an instability to form the Rabi force peaks together with the phase inflections. Such an instability makes a transition between the two slow manifolds with different winding numbers easier: Once the phase inflections are formed together with the Rabi force peaks, such structures persist on a quite long time scale although the heights of the Rabi force peaks are modulated chaotically on the time scale of the mode partition noise. Further the 'loop' structure illustrated in Fig. 9(b), which enables the mode hopping, always grows from one of the phase inflections. These facts mean that a low dimensional path through which topological property likely changes is self-formed with a long lifetime in the infinite dimensional phase space. Attempts to change the winding number are repeated along the path, and the attempt is successfully achieved, when the Rabi force is occasionally strong enough.

The persistent phase inflections, on the other hand, makes the phase derivative spatially quite inhomogeneous, which means that the central modes with mode number other than the winding number are excited (see Eq. (4·5a)). This is the origin of the multiple modes firing state mentioned above. Thus, the multi-mode firing and the formation of the path between the localized attractors is closely connected with each other. The persistent structures, which is observed as the multi-mode photon number distribution, is not determined by the winding number alone; it being dependent upon the past history of hopping experienced by the system.

The interplay between the central range and the Rabi chaotic bands seems to be essential for the mode hopping to be self-induced. Indeed, if we transplant random variables decorrelated with the state of the central range to the Rabi chaotic bands of system II, clear transitions between well defined winding numbers cannot be realized even if the random variables are constructed so as to replicate the statistical property

of the modes in the Rabi bands. The Rabi force is not a simple random force generated independent of the state of the system; it being an 'internal force' which is formed with a strong correlation with the past evolution of the central range. The internal force generated through a chaotic evolution of the system itself seems to be more effective than the externally applied random force in searching for the paths through which the itinerancy over the attractor ruins is realized. A more qualitative analysis of such a process will be presented in a forthcoming publication.

## § 5. Discussion

In the present paper we have investigated in detail complex dynamical behaviors of multi-mode oscillation exhibited by the Maxwell-Bloch (M-B) equation, confining ourselves to the good cavity case. The symmetry of the M-B system imposes a simple topological constraint on the structure of the slow manifold of the system, and hence the single mode stationary solutions (SSSs) which are stable when the pumping parameter is small enough are characterized by the winding number. Any SSS undergoes instability leading to a self-oscillation of the Rabi precession when the pumping parameter exceeds a threshold value. With further increase in the pumping parameter, the Rabi precession becomes chaotic, and the chaotic attractors, each of which has been localized in the phase space around a SSS with a definite winding number, further merge into a global attractor. It is such a globally chaotic motion that we investigated in detail in the present paper. The global chaos is contributed by a large number of cavity modes, and it provides a typical example of complex dynamics in nonlinear optical systems.

First we investigated how information carried by chaotic disturbances is generated and propagates in the wave-number space. The 2-point and the 3-point mutual information (MI) are computed in order to clarify the information structure formed in the wave-number space. More than 90% of electromagnetic energy is distributed to the wave-number region nearly resonant with the two level medium (we call this the central range), but chaotic information is generated in two narrow wave-number regions called the Rabi chaotic bands which are symmetric with respect to the central range. Each of the two bands splits further into the two regions which we call the upper band and the lower band, and the two information networks originating from each of the two regions are formed in the wave-number space: The upper band controls the motion in the higher-harmonic regions of the Rabi unstable bands, whereas the lower band governs the dynamics in the regions between the neighbouring higher-harmonic regions. In any way the sources of turbulent motion are in the two Rabi chaotic bands.

The information theoretical study further reveals that the dynamics in the central range has a time scale much longer than that of the chaotic motion. Such a slow motion in the central range, however, severely influences the motion in the Rabi chaotic bands. Moreover, the sudy of the 3-point MI indicates that a correlated motion is activated among the two Rabi chaotic bands and the central range. Therefore, the rapidly varying chaotic motion in the Rabi bands is influenced considerably by the slowly varying motion in the central range, and vice versa. We have

to, however, emphasize that the central range does not directly contribute to generating chaotic information.

The interplay between the Rabi chaotic bands and the central range results in physically interesting phenomena. First the scattering process between the two Rabi chaotic bands yields low wave-number fluctuations which vary rapidly on the chaotic time scale. Such fluctuations perturb the central modes, and the photon number of each of the central modes fluctuates significantly although the total number of photons in the central range is almost conserved. This phenomenon corresponds to the mode partition noise which has been often observed in the multi-mode laser oscillations. The mode partition noise has been understood in terms of the photon number dynamics driven by an externally applied noise. However, the mode partition noise in our system is due to the chaotic motion excited in the Rabi chaotic bands, and furthermore the topological constraint inherent in the M-B system plays a crucial role. It is a slowly varying fluctuation of a phase variable associated with a spatial structure with a given winding number. The time scale of the mode partition noise is much longer than the time scale of chaotic motion in the Rabi bands and is proportional to the square of the system size.

On a time scale still much longer than that of the mode partition noise, sudden transitions through which the winding number changes take place. At each transition a drastic change occurs in the distribution of photon numbers over the central modes. This phenomenon corresponds to the mode hopping which has been observed for multi-mode laser oscillations. We have to note that the origin of mode hopping in the M-B system is not the external noise decorrelated with the state of the system. It owes to chaotic motion generated by the system itself, and the chaotic dynamics seems to work more effectively than the externally applied random force in realizing the mode hopping. Indeed we showed that the Rabi chaotic bands and the central range work cooperatively and eventually lead to an instability through which an easy path connecting the two states with different winding numbers is self-generated. Such an easy path has a quite long lifetime, and the chaotic force originating from the Rabi bands makes the central range attempt to change the winding number through the self-generated easy path. If such an attempt is achieved successfully, a similar process mentioned above will be repeated once again at the new state. In such a way an endless itinerancy over the ruins of local attractors is realized.

As has been mentioned, an example of chaotic itinerancy wandering over multiple attractor ruins was reported for a model of passive bistable resonator,[9] and it is recently reconsidered by Davis in the context of the chaotic memory search problem.[30] The fact that chaos works more effectively than externally applied random force in inducing a hopping among local attractors suggests a possibility that a new scheme of memory search may be deviced by employing chaotic dynamics. From this standpoint, the recent experiment reported by Anderson and Erie[5] is quite interesting. They observed an itinerancy phenomenon with a holographic resonator which works as an associative memory element, and they called it 'day dream'. In this case the itinerancy is a mode hopping among the memories which correspond to the single mode stationary states in our M-B system. It is, however, still unclear whether the origin of mode hopping is attributed to a deterministic chaos or not. Itinerancy over

the memories due to the 'noise-induced' chaos has been predicted theoretically by Tsuda for a neural network system modeling a dynamical aspect of the brain.[31] A chaotic wandering over long-lived coherent structures is reported quite recently by Kaneko for his globally coupled map lattice model which may be regarded as a nonequilibrium version of the Hopfield model.[32] Anyhow, examples of the chaotic itinerancy are found in a wide area of physical science, and systematic studies on it are strongly desired.

## References


1) T. H. Maiman, Nature **187** (1960), 463.
V. Etuhov and J. K. Neeland, *Pulsed Ruby Lasers*, ed. A. K. Levine (Marcel Dekker, N. Y., 1966), chap. 1.
2) See, for example,
T. Gotoh, A. Arimoto, M. Ojima and N. Chinone, SPIE, 329, Optical Disk Technology (1982), 56;
N. Chinone, T. Kuroda, T. Otsuka, T. Takahashi and T. Kajimura, IEEE J. Quantum Elecron. **QE-21** (1985), 1264.
See also Ref. 29).
3) M. S. Borisova and V. M. Yasinskii, Opt. and Spectrosc. **31** (1971), 231.
K. Otsuka, 'Ultra-fast optical pulse generation in Nd-YAG lasers,' Ph. D. thesis, Tohoku University (1976).
K. Kuroda, Phys. Rev. **A19** (1979), 231.
L. A. Melnikov, E. M. Rabinovich and V. V. Tuchin, J. Opt. Soc. Am. **B5** (1988), 1134.
D. L. MacFarlane, L. W. Casperson and A. A. Tavor, J. Opt. Soc. Am. **B5** (1988), 1144.
4) See, for example, R. Lang and K. Kobayashi, IEEE J. Quantum Electron. **QE16** (1980), 347.
5) See for example, D. Z. Anderson and M. C. Erie, Optical Engineering **26** (1987), 434.
6) K. Ikeda, Opt. Commun. **30** (1979), 257.
K. Ikeda, H. Daido and O. Akimoto, Phys. Rev. Lett. **45** (1980), 709.
K. Ikeda, *Coherence and Quantum Optics V*, ed. L. Mandel and E. Wolf (Plenum, N. Y., 1984), p. 875.
7) H. M. Gibbs, *Optical Bistability: Controlling Light with Light* (Academic Fress, Orlando, 1985), chap. 6.
8) See, for example, articles in *Instabilities and Chaos in Quantum Optics,* ed. F. T. Arecchi and R. G. Harrison (Springer-Verlag, Berlin, 1987).
9) K. Ikeda and K. Matsumoto, J. Stat. Phys. **44** (1986), 955; Physica **29D** (1987), 223.
10) See, for example, articles in *Optical Instabilities,* ed. R. Boyd et al. (Cambridge Univ. Press, Cambridge, 1985).
11) For instability and chaos in active optical systems see, for example, J. Opt. Soc. Am. **B2** (1985), No. 1 and J. Opt. Soc. Am. **B5** (1988), No. 5.
12) K. Ikeda and K. Matsumoto, Phys. Rev. Lett. **62** (1989), 2265.
13) See, for example,
A. S. Bashkin et al., Sov. J. Quantum Electron. **1** (1971), 146;
M. D. Sayers and L. Allen, Phys. Rev. **A1** (1970), 1730;
K. Otsuka, IEEE J. Quantum Electron. **QE-14** (1978), 1007.
14) L. W. Casperson, IEEE J. Quantum Electron. **QE-14** (1978), 756.
15) P. Mandel, Ref. 8), p. 263.
16) H. Risken and K. Nummendal, J. Appl. Phys. **39** (1968), 4462.
H. Risken, Ref. 8), p. 20.
17) C. O. Weiss, N. B. Abraham and U. Hüber, Phys. Rev. Lett. **61** (1988), 1587.
18) M. Mayer, H. Risken and H. D. Vollmer, Opt. Commun. **36** (1981), 480.
L. A. Lugiato, L. M. Nurducci, E. V. Eschenazi, D. K. Bandy and N. B. Abraham, Phys. Rev. **A32** (1985), 1563.
T. Ogawa, Appl. Phys. **B49** (1989), 397.
19) W. Brunner, R. Fisher and H. Paul, J. Opt. Soc. Am. **B2** (1985), 202.

20) M. Sargent III, M. O. Scully and W. E. Lamb, Jr., *Laser Physics* (Addison-Wesley, Reading, 1974), chaps. IX and XI.
21) P. G. Gerber and M. Büttiker, Z. Phys. **B33** (1979), 219.
22) R. Graham and H. Haken, Z. Phys. **213** (1968), 420.
23) K. Matsumoto and I. Tsuda, Physica **26D** (1987), 347; J. of Phys. **A21** (1988), 1405.
24) C. E. Shannon and W. Weaber, *The Mathematical Theory of Communication* (Univ. Illinois Press, Urbana, 1949).
R. J. McEliece, *The Theory of Information and Coding* (Addison-Wesley, Reading, 1977).
25) MI map has been used to clarify the information flow in a simple biological system, K. Matsumoto, T. Ueda and K. Kobatake, in preparation.
26) L. W. Hillman, J. Krasinski, R. W. Boyd and C. W. Stroud, Jr., Phys. Rev. Lett. **53** (1984), 1605.
27) See, for example,
T. Suzuki, J. Appl. Phys. **41** (1970), 3904;
T. Ito, S. Machida, K. Nawata and T. Ikegami, IEEE J. Quantum Electron. **QE13** (1977), 574.
28) See, for example,
G. Arnold and K. Peterman, Opt. Quantum Electron. **12** (1980), 207;
S. E. Miller and D. Marcuse, IEEE J. Quantum Electron. **QE20** (1984), 1032.
29) M. Ohtsu, Y. Teramachi, Y. Otsuka and A. Osaki, IEEE J. Quantum Electron. **QE22** (1986), 535.
30) P. Davis, submitted to Phys. Rev. **A**.
P. Davis and K. Ikeda, to appear in Phys. Rev. **A**.
31) I. Tsuda, to be published in *Neurocomputers and Attention* (1990), ed. V. I. Kryukov et al.
32) K. Kaneko, to appear in Physica **D**.